

Results from the ARGO-YBJ Test Experiment

The ARGO-YBJ Collaboration*

Presented by M. Iacovacci ^a

^aDipartimento di Fisica dell'Università di Napoli and I.N.F.N., Napoli, Italy

An RPC carpet covering $\sim 10^4 m^2$ (ARGO-YBJ experiment) will be installed in the YangBaJing Laboratory (Tibet, P.R. China) at an altitude of 4300 m a.s.l.. A test-module of $\sim 50 m^2$ has been put in operation in this laboratory and about 10^6 air shower events have been collected. The carpet capability of reconstructing the shower features is presented.

1. INTRODUCTION

The ARGO-YBJ experiment is under way over the next few years at Yangbajing High Altitude Cosmic Ray Laboratory (4300 m a.s.l., 606 g/cm²), 90 km North to Lhasa (Tibet, P.R. China). The aim of the experiment is the study of cosmic rays, mainly cosmic γ -radiation, at an energy threshold of $\sim 100 GeV$, by means of the

detection of small size air showers at high altitude. The apparatus consists of a full coverage detector of dimension $\sim 71 \times 74 m^2$ realized with a single layer of Resistive Plate Counters (RPCs). The area surrounding the central detector core, up to $\sim 100 \times 100 m^2$, consists of a guard ring partially ($\sim 50\%$) instrumented with RPCs. These outer detector improves the apparatus performance, enlarging the fiducial area, for the detection of showers with the core outside the full coverage carpet. A lead converter 0.5 cm thick will cover uniformly the RPC plane in order to increase the number of charged particles by conversion of shower photons and to reduce the time spread of the shower front. The site location (longitude 90° 31' 50" E, latitude 30° 06' 38" N) permits the monitoring of the Northern hemisphere in the declination band $-10^\circ < \delta < 70^\circ$.

Such a detector, performing a continuous high sensitivity sky survey, complements the narrow field of view air Cerenkov telescopes allowing to bridge the GeV and TeV energy regions and to face a wide range of fundamental issues in Cosmic Ray and Astroparticle Physics including γ -ray astronomy, GRBs physics and the measurement of the \bar{p}/p at TeV energies [1]. Detector assembling will start late in 2000 and data taking with the first $\sim 750 m^2$ of RPCs in 2001.

In order to investigate both the RPCs performance at 4300 m a.s.l. and the capability of the detector to sample the shower front of atmospheric cascades, during 1998 a full coverage carpet of $\sim 50 m^2$ has been put in operation in the

*C. Bacci¹, K.Z. Bao², F. Barone³, B. Bartoli³, P. Bernardini⁴, S. Bussino¹, E. Calloni³, B.Y. Cao⁵, R. Cardarelli⁶, S. Catalanotti³, A. Cavaliere⁶, S. Cavaliere³, F. Cesaroni⁴, P. Creti⁴, Danzengluobu⁷, B. D'Ettoe Piazzoli³, M. De Vincenzi¹, T. Di Girolamo³, G. Di Sciascio³, Z.Y. Feng⁸, Y. Fu⁵, X.Y. Gao⁹, Q.X. Geng⁹, H.W. Guo⁷, H.H. He¹⁰, M. He⁷, Q. Huang⁸, M. Iacovacci³, N. Iucci¹, H.Y. Jai⁸, F.M. Kong⁵, H.H. Kuang¹⁰, Labaciren⁷, B. Li², J.Y. Li⁵, Z.Q. Liu⁹, H. Lu¹⁰, X.H. Ma¹⁰, G. Mancarella⁴, S.M. Mari¹¹, G. Marsella⁴, D. Martello⁴, D.M. Mei⁷, X.R. Meng⁷, L. Milano³, A. Morselli⁶, J. Mu⁹, M. Panarco⁴, Z.R. Peng¹⁰, P. Pistilli¹, R. Santonic⁶, P.R. Shen¹⁰, C. Stanescu¹, J. Su¹⁰, L.R. Sun², S.C. Sun², A. Surdo⁴, Y.H. Tan¹⁰, S. Vernetto¹², C.R. Wang⁵, F. Wang¹⁰, H.Y. Wang¹⁰, Y.N. Wei², H.T. Yang⁹, Q.K. Yao², G.C. Yu⁸, X.D. Yue², A.F. Yuan⁷, H.M. Zhang¹⁰, J.L. Zhang¹⁰, N.J. Zhang⁵, T.J. Zhang⁹, X.Y. Zhang⁵, Zhaxisangzhu⁷, Zhaxiciren⁷, Q.Q. Zhu¹⁰. ¹ INFN and Dipartimento di Fisica dell'Università di Roma Tre, Italy, ² Zhengzhou University, Henan, China, ³ INFN and Dipartimento di Fisica dell'Università di Napoli, Italy, ⁴ INFN and Dipartimento di Fisica dell'Università di Lecce, Italy, ⁵ Shandong University, Jinan, China, ⁶ INFN and Dipartimento di Fisica dell'Università di Roma "Tor Vergata", Italy, ⁷ Tibet University, Lhasa, China, ⁸ South West Jiaotong University, Chengdu, China, ⁹ Yunnan University, Kunming, China, ¹⁰ IHEP, Beijing, China, ¹¹ Università della Basilicata, Potenza, Italy, ¹² Istituto di Cosmofisica del CNR and INFN, Torino, Italy

YangBaJing (YBJ) Laboratory. Results concerning both the RPCs behaviour and the features of the showers imaged by the carpet are presented.

2. THE EXPERIMENTAL SET-UP

The set-up of the detector is an array of 3×5 chambers of area $280 \times 112 \text{ cm}^2$ each, covering a total area of $\sim 8.6 \times 6.0 \text{ m}^2$. The active area of $\sim 45.8 \text{ m}^2$, accounting for a dead area due to a 7 mm frame closing the chamber edge, corresponds to a $\sim 89\%$ coverage. The RPCs, with a 2 mm gas gap, are built with bakelite electrode plates of volume resistivity in the range $(0.5 \div 1) 10^{12} \Omega \cdot \text{cm}$. The RPC signals are picked up by means of aluminum strips 3.3 cm wide and 56 cm long which are glued on a 0.2 mm thick film of Poly-Ethylen-Tereftalate (PET). At the edge of the detector the strips are connected to the front-end electronics and terminated with 50Ω resistors. A grounded aluminum foil is used to shield the bottom face of the RPC and an extra PET foil, on top of the aluminum, is used as a further high voltage insulator. The front-end circuit contains 16 discriminators, with about 50 mV voltage threshold, and provides a FAST-OR signal with the same input-to-output delay (10 ns) for all the channels. This signal is used for time measurements and trigger purposes in the present test. The 16 strips connected to the same front-end board are logically organized in a pad of $56 \times 56 \text{ cm}^2$ area. Each RPC is therefore subdivided in 10 pads which work like independent functional units. The pads are the basic elements ("pixel") which define the space-time pattern of the shower; they give indeed the position and the time of each detected hit. At any trigger occurrence the times of all the pads are read-out by means of multihit TDCs of 1 ns time bin, operated in common STOP mode. Since the pad signal is shaped to $1.5 \mu\text{s}$, only the time profile of the earliest particles hitting the pads is imaged. The set-up was completed with a small telescope consisting of 3 RPCs of $50 \times 50 \text{ cm}^2$ area with 16 pick-up strips 3 cm wide connected to front-end electronics board similar to the ones used in the carpet. The 3 RPCs were overlapped one on the other and the triple coincidence of their FAST-

OR signals was used to define a cosmic ray crossing the telescope.

3. RPC PERFORMANCE

The RPCs were operated in streamer mode as foreseen for the final experiment. This mode delivers large amplitude saturated signals and is less sensitive than the avalanche or proportional mode to electromagnetic noise, to changes in the environment conditions and to mechanical deformations of the detector. Three gas mixtures

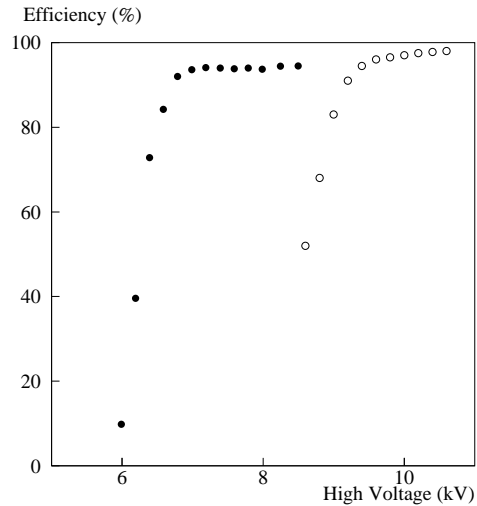


Figure 1. Detection efficiency *vs* operating voltage for one of the carpet RPCs (●). The same curve for a 2 mm gap RPC operating at sea level is also reported (○) for comparison.

were tested which used the same components, Argon, Isobutane and TetraFluoroEthane, in different proportions: TFE/Ar/i-But = 45/45/10; 60/27/13 and 75/15/10. An higher TFE concentration in place of the Ar concentration increases the primary ionization thus compensating for the 40% reduction caused by the lower gas target pressure (600 mbar) and reduces the

afterpulse probability. The reduction of the Argon concentration in favour of TFE results in a clear increase of the operating voltage as expected from the large quenching action of TFE. Since the higher the TFE fraction, the lower is the charge delivered in the gas by a single streamer, we decided to operate the test carpet with the gas mixture corresponding to the highest TFE fraction, in order to extend the dynamic range achievable for the analogical read-out.

Fig. 1 shows the operating efficiency for 4 ORed pads. The efficiency was measured using cosmic ray signals defined by means of an auxiliary telescope placed on top of the carpet. The same curve for a 2 mm gap RPC operated at sea level is also shown for comparison. The detection efficiency *vs* operating voltage, compared to the operation at 606 mbar pressure in YBJ, shows an increase of ~ 2.5 kV in operating voltage. The effect of small changes in temperature T and pressure P on the operating voltage can be accounted for by rescaling the applied voltage V_a according to the relationship:

$$V = V_a \frac{P_0}{P} \cdot \frac{T}{T_0} \quad (1)$$

where P_0 and T_0 are arbitrary standard values, e.g. 1010 mbar and 293 K respectively for a sea level laboratory. This formula predicts, starting from the YBJ data, an operating voltage at sea level which is considerably smaller than the experimental one. However, a good consistency is recovered by assuming that, in the ideal gas approximation, the parameter which fixes the operating voltage is given by *gap · pressure / temperature*. Measurements on RPCs with different gas gap size justify this assumption.

Fig. 1 also shows that the plateau efficiency measured at YBJ is $3 \div 4\%$ lower than at the sea level. Although a lower efficiency is expected from the smaller number of primary clusters at the YBJ pressure, we attribute most of the difference to the underestimation of the YBJ efficiency. At YBJ altitude, indeed, the ratio of the cosmic radiation electromagnetic to muon component is ~ 4 times larger than at sea level. A spatial tracking with redefinition of the carpet track downstream would eliminate the contamination

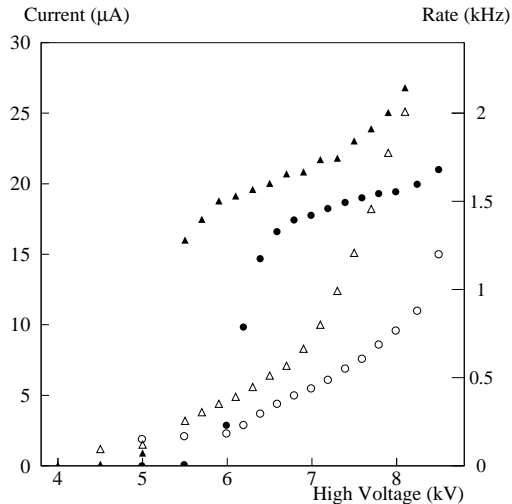


Figure 2. Counting rate (full symbols) and operating current (open symbols) vs Voltage of one RPC of the carpet. Results are presented for two different TFE percentages (45%:triangles and 75%:circles). The rate shown refers to 4 of the 10 ORed RPC pads.

from soft particles, giving a more accurate and higher efficiency. On the other hand the lower efficiency could hardly be explained with the gas lower density. In fact, the number of primary clusters in the YBJ test, estimated around 9, is the same as in the case of some gas, e.g. Ar/i-But/CF₃Br = 60/37/3, that was frequently used at sea level with efficiency of $\sim 97 \div 98\%$.

The counting rate of 4 ORed pads, together with the RPC current, are reported in Fig. 2 *vs* the operating voltage. The results for a percentage of 45% of TFE are also reported for comparison. A rather flat singles counting rate plateau is observed at a level of ~ 400 Hz for a single pad of area 56×56 cm².

The time jitter distribution of the pad signals was obtained by measuring the delay of the FAST-OR signal with respect to RPC2 (the RPC in the central position of the trigger telescope) by means of a TDC with 1 ns time bin. This distri-

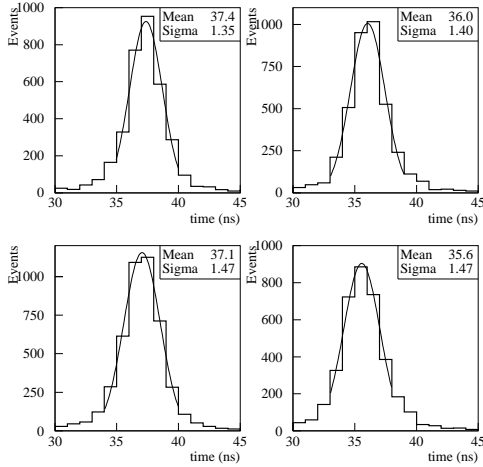


Figure 3. Time jitter distribution of 4 pads of the carpet. The telescope RPC2 signal is used as common stop.

bution is shown in Fig. 3 for four pads. The average of the standard deviations is 1.42 ns corresponding to a resolution of $\sim 1 \text{ ns}$ for the single RPC if we account for the fact that the distributions show the combined jitter of two detectors. A more detailed presentation of these results is reported in [2].

4. DATA ANALYSIS OF SHOWER EVENTS

Data were taken either with or without a 0.5 cm layer of lead on the whole carpet in order to investigate the converter effect on multiplicity and angular resolution. A trigger based on pad multiplicity has been used to collect $\sim 10^6$ shower events in April-May 1998. The integral rate as a function of the pad multiplicity is shown in Fig. 4 for showers before and after the lead was installed. A comparison at fixed rate indicates an increase of pad multiplicity due to the effect of the lead of $\sim 15 \div 20\%$, as expected according to our simulations. Since in this test the strip

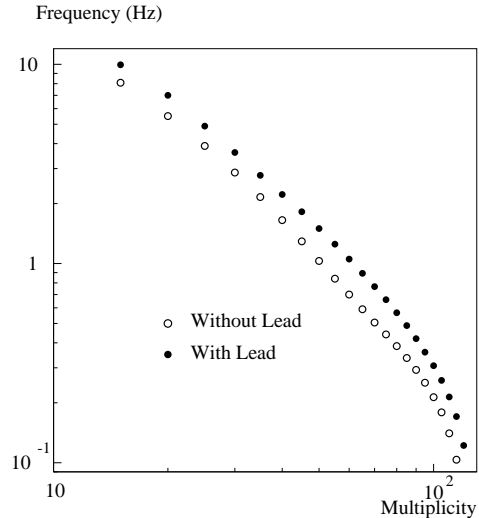


Figure 4. The integral rate as a function of the pad multiplicity.

read-out is not effective, the actual multiplicity is underestimated for particle densities higher than $\sim 1 \text{ m}^{-2}$. Data have been corrected to obtain the average particle density as a function of the recorded multiplicity (Fig. 5).

4.1. Event reconstruction

Due to the reduced size of the detector, the time profile of the shower front sampled by the carpet is expected to exhibit a planar shape. In this approximation the expected particle arrival time is a linear function of the position. We performe an optimized reconstruction procedure of the shower direction as follows:

- Unweighted plane fit to hits for each event by minimization of the function

$$\chi^2 = \frac{1}{c^2} \sum_i \{lx_i + my_i + nz_i - c(t_i - t_0)\}^2 \quad (2)$$

The sum includes all counters with a time signal t_i , c is the light velocity, (x_i, y_i, z_i) are the i th center pad position coordinates. The parameters of the fit are the time offset t_0 and the l, m direction cosines.

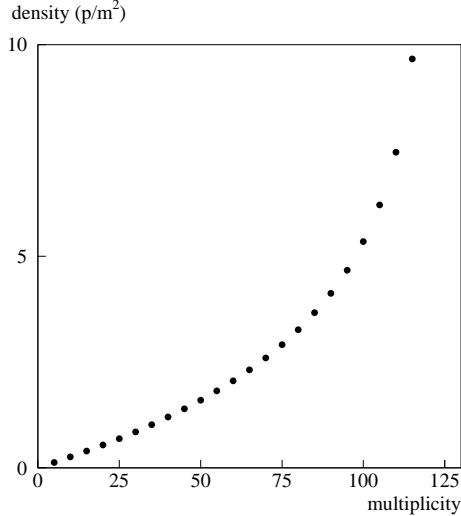


Figure 5. The particle density as a function of the measured multiplicity.

- Rejection of outlying points by means of a $K \cdot \sigma$ cut and iteration of the fit until all points verify this condition. If the remaining hits number is ≤ 5 the event is rejected. Here σ is the standard deviation of the distribution.

This procedure is rather fast because it makes use only of analytic formulae. No *a priori* information about shower features is required. The actual value of K could depend on the features of the reconstructed showers as well as on the experimental conditions (pad dimension, shaping of the signals, multihit capability, etc.). By choosing $K = 2.5$ about 8% of the hits are rejected. Increasing K should increase the number of discarded hits without a significant improvement of the χ^2 . The χ^2 distribution exhibits a long tail more pronounced for low multiplicity events. In these high χ^2 events the time hits are considerably spread, by far more than expected from the detector time resolution. They can be attributed to the sampling of a portion of the shower affected by large time fluctuations. Events with reduced $\chi^2 > 30 \text{ ns}^2$ ($\sim 10\%$ of the total) have been dis-

carded and not used in the following analysis.

4.2. The zenith angle distribution

Since the shower size is not measured, events have been classified according to the observed particle density. The zenith angle distribution of the integral density spectrum is expected to follow an exponential behaviour

$$I(\geq \rho, \theta) = I(\geq \rho, 0) \cdot e^{-\frac{x_0}{\Lambda_{att}}(\sec\theta - 1)} \quad (3)$$

where x_0 is the vertical depth. The attenuation mean free path Λ_{att} of EAS is related to the absorption length Λ_e of EAS particles by $\Lambda_{att} = \Lambda_e/\gamma$ where γ is the index of the integral density spectrum. The angular distribution of events with density greater than 3.0 particles/ m^2 (corresponding to $N_{hit}(\theta) = 76 \cdot \cos\theta$) is shown in Fig. 6. The data can be fit out to $\sim 55^\circ$ with

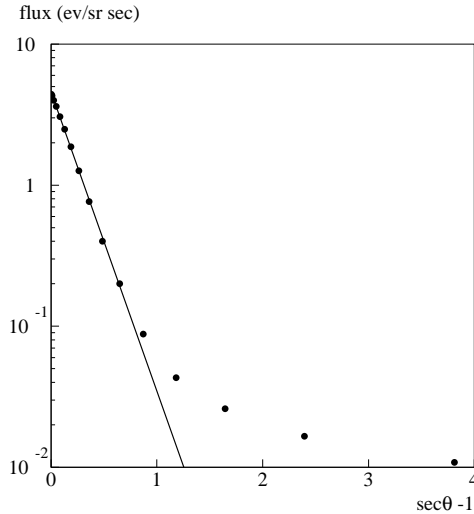


Figure 6. The zenith angle distribution.

an $\exp[-\alpha \cdot (\sec\theta - 1)]$ law. The parameter α is found to be 4.88 ± 0.45 , so that $\Lambda_{att} = (124 \pm 11) \text{ g/cm}^2$, in excellent agreement with previous results concerning the density spectrum of shower

particles [3]. For angles greater than 55° a deviation from this law is observed. Misreconstructed events, showers locally produced in the walls of the surrounding buildings and horizontal air showers could contribute to these large angle events. This result is substantially unchanged for densities ranging from 1 to 5 particles/ m^2 .

Data confirm that the shape of the angular distribution is dominated by the physical effect of atmospheric absorption and that no relevant instrumental effects or selection biases have been introduced.

4.3. The density spectrum

The differential density spectrum measured in three different intervals of zenith angles is shown in Fig. 7. The angular bin size is $\Delta\theta = 5^\circ$, so that the difference of atmospheric depth inside the source bin is $\leq 40 \text{ g/cm}^2$ (about one radiation length) for zenith angles up to 35° . A smaller bin

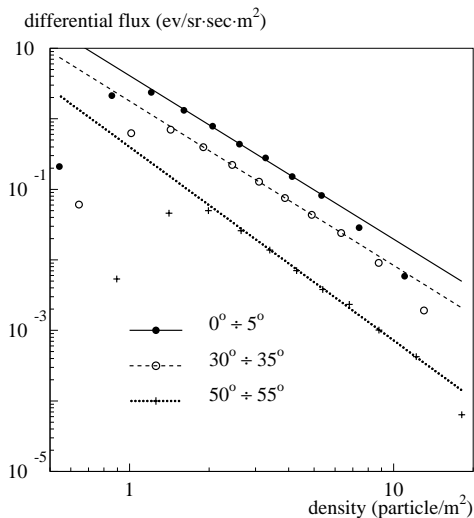


Figure 7. Differential density spectrum for three intervals of zenith angle.

size has been used to analyze data up to 55° . The spectra refer to the depth corresponding to the

mean zenith angle of the showers recorded inside each interval. The shapes of the spectra are very similar in the density range $2 \div 8 \text{ particles/m}^2$ not affected by threshold or saturation effects.

The index γ_d of the density spectrum as a function of the zenith angle is shown in Fig. 8. A weighted mean up to $\theta < 45^\circ$ gives 2.33 ± 0.03 . This value is fully consistent with the ones obtained in experiments at high altitude at comparable particle densities [4]. MonteCarlo simulations show that present data concern energies ranging from about 1 TeV (quasi-vertical showers) to a few hundred TeV ($\theta \sim 45^\circ$). Accordingly, the measured γ_d can be considered a reasonable estimate of the slope of the density spectrum of showers initiated by primaries (mainly protons) of energies $\sim 10^{13} \div 10^{14} \text{ eV}$. From these data the absorption length of EAS particles Λ_e is found to be $165 \pm 18 \text{ g/cm}^2$ consistent with results of similar measurements at small shower sizes [3]. Data recorded at large zenith angles ($> 45^\circ$) are due to showers developed through atmospheric depths greater than 860 g/cm^2 . Thus, a substantial contribution is expected from showers originated by primaries of energies beyond the knee of the cosmic ray spectrum. This could explain the increasing of the slope γ_d with zenith angle, as shown in Fig. 8.

4.4. Shower front thickness

The time distribution of the shower hits with respect to the fitted plane is shown in Fig. 9 for two different multiplicity ranges. Quasi-vertical showers ($\theta < 15^\circ$) have been selected. The distribution of time residuals exhibits, as expected, a long tail due to time fluctuations and to the curved profile of the shower front, more pronounced for low multiplicity. The width of these distributions is related to the time thickness of the shower front. Since the position of the shower core is not reconstructed, the experimental result concerns a time thickness averaged on different radial distances.

For low multiplicity events with a mean number of particles per pad < 1 , the spread σ represents a reasonable measurement of the shower thickness. For high multiplicity events ($N_{hit} > 100$), where the mean number of particles hitting one pad is

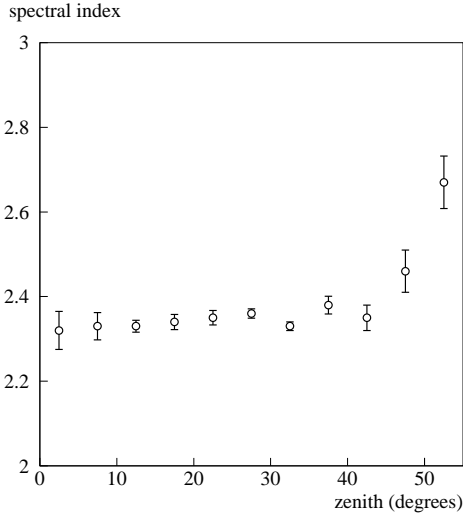


Figure 8. The index γ_d of the density spectrum as a function of the zenith angle.

> 1 , this σ does not express the thickness of the shower disc without any bias. In fact, the time residual distribution is related to the fluctuations of the first particle detected by each pad. Taking into account the total detector resolution of 1.3 ns (RPC intrinsic jitter, strip length, electronics time resolution) the time jitter of the earliest particles in high multiplicity events (> 100 hits) is estimated $\sim 1 \text{ ns}$. The averaged shower front thickness of low multiplicity events (particle density $< 1 \text{ m}^{-2}$) is found $\sim 4.4 \text{ ns}$.

4.5. Angular resolution

The angular resolution of the carpet has been estimated by dividing the detector into two independent sub-arrays ("odd pads" and "even pads") and comparing the two reconstructed shower directions. These two sub-arrays overlap spatially so that they are affected by the same shower curvature. Events with total number of hits N_{hit} have been selected according to the constraint $N_{odd} \simeq N_{even} \simeq N_{hit}/2$. The distribution of the even-odd angle difference $\Delta\theta_{eo}$ is shown in Fig. 10 for events in different multiplicity ranges and

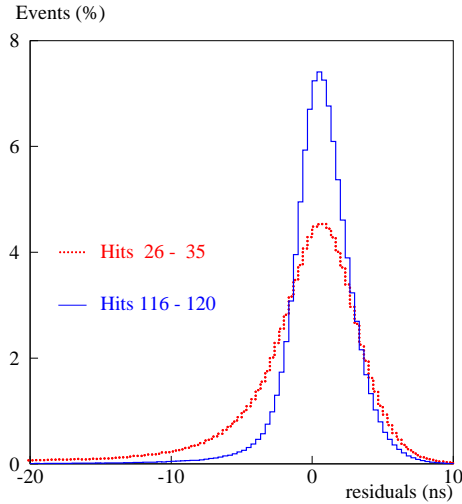


Figure 9. Distribution of time residuals for events with different pad multiplicity (all channel added).

$\theta < 55^\circ$. These distributions narrow, as expected, with increasing shower size.

The effect of the lead sheet on the angular resolution can be appreciated in Fig. 11, where the median $M_{\Delta\theta_{eo}}$ of the distribution of $\Delta\theta_{eo}$ as a function of pad multiplicity, for showers reconstructed before and after the lead was added, is shown. The improvement of the angular resolution is a factor ~ 1.4 for $N_{hit} = 50$ and decreases with increasing multiplicity. Assuming that the angular resolution function for the entire array is Gaussian, its standard deviation σ is given by [5] $\sigma_\theta = \frac{M_{\Delta\theta_{eo}}}{1.177 \times 2}$. This chessboard method yields a standard deviation $\sigma_\theta \sim 2.1^\circ$ for events with a pad multiplicity ≥ 100 .

5. CONCLUSIONS

A carpet of $\sim 50 \text{ m}^2$ of RPCs has been put in operation at the Yangbajing Laboratory in order to study the high altitude performance of RPCs and the detector capability of imaging with high granularity a small portion of the EAS disc, in

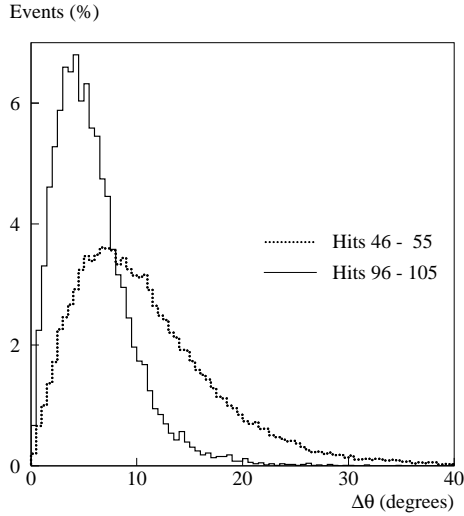


Figure 10. Even-odd angle difference distribution for events with different pad multiplicity.

view of an enlarged use in Tibet (ARGO-YBJ experiment).

The results of this test confirm that RPCs can be operated efficiently ($\geq 95\%$) to sample air showers at high altitude with excellent time resolution (~ 1 ns). The analysis of data collected with a shower trigger suggest that the RPCs carpet capability of reconstructing the shower features is consistent with expectations. As a conclusion, the overall results of the test look well promising for future operation of the full detector.

REFERENCES

1. Abbrescia M. et al., *Astroparticle Physics with ARGO*, Proposal (1996).
Download this document at the URL: www1.na.infn.it/wsubnucl/cosm/argo/argo.html
2. Bacci C. et al., submitted to Nucl. Instr. Meth. (1999).
3. Bennet S. et al., J. Phys. Soc. of Japan, Vol. 17 Supp. A-III (1961) 196.
4. Greisen K., Progr. Cosmic Ray Physics, Vol.

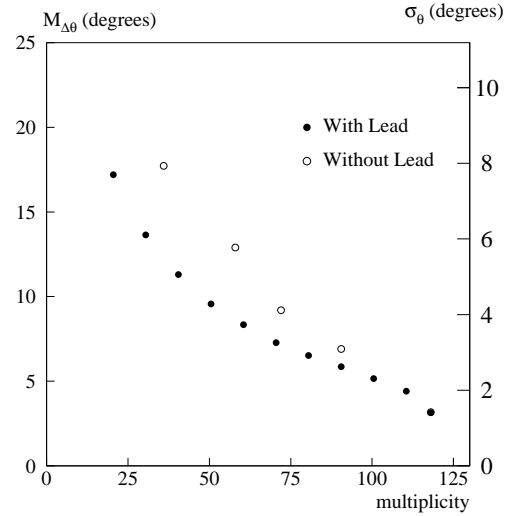


Figure 11. Median of $\Delta\theta_{eo}$ distribution as a function of pad multiplicity.

III (1956).

5. Alexandreas D.E. et al., Nucl. Instr. Meth. A311 (1992) 350.